Acta Neuropathologica (2026) 151:54
https://doi.org/10.1007/s00401-026-03026-1

ORIGINAL PAPER

Molecular profiling of alpha-synuclein pathology and seeding activity in Parkinson's disease

Zeynep Bengisu Kaya[1] · Danilyn Amerna[1] · Ananya Susarla[1] · Melina J. Lim[1] · Maria Bregendahl[1,2] · Hiroaki Sekiya[1] · Michael DeTure[1] · Owen A. Ross[1,2] · Dennis W. Dickson[1,2] · Suelen L. Boschen[1,2] · Pamela J. McLean[1,2]

Received: 30 December 2025 / Revised: 26 April 2026 / Accepted: 1 May 2026

Abstract

Parkinson's disease (PD) is neuropathologically characterized by the abnormal accumulation of fibrillar alpha-synuclein (aSyn) within selectively vulnerable neuronal populations. Although this pathological hallmark is shared across individuals with PD, the disease presents with marked clinical heterogeneity in age of onset, progression rate, and clinical symptoms, the molecular basis of which remains incompletely understood. In this study, we examined whether biochemical and seeding-related properties of aSyn vary across clinically defined PD subgroups. Using well-characterized, autopsy-confirmed PD cases and matched controls we applied complementary biochemical, cell-based aggregation, and cell-free seed amplification assays (SAA) to investigate aSyn molecular heterogeneity and its potential contribution to disease diversity. Autopsy-confirmed PD cases were classified as early-onset (< 60 years) or late-onset (> 60 years), with the late-onset group further subdivided into fast-progressing (< 5 years duration) and slow-progressing (> 10 years duration). Analysis of detergent-insoluble fractions from PD brains revealed significantly elevated pSer129-aSyn levels compared to controls, while total aSyn was highest in late-onset PD. Seeding bioactivity measured via FRET-based biosensor cells was significantly increased in PD, albeit with substantial inter-individual variability; late-onset and slow-progressing groups exhibited the strongest activity. Seeding activity correlated positively with pSer129-aSyn levels. These findings were supported by high-content imaging, which demonstrated increased intracellular aggregate burden in PD samples. SAA confirmed robust seeding activity in PD, with shorter lag times relative to controls. Finally, proteinase K digestion of amplified products revealed differences in proteolytic resistance between PD and control samples, consistent with biochemical heterogeneity of seeding-competent species. Collectively, these findings suggest that aSyn pathology in PD is associated with marked inter-individual variability in biochemical and seeding properties. Our results highlight the importance of considering molecular heterogeneity at the individual patient level when investigating PD pathobiology and supports the need for precision medicine approaches for PD patients.

Keywords Parkinson's disease · Alpha-synuclein · Seeding · FRET · SAA

Abbreviations

AlphaLISA	Amplified Luminescent Proximity Homogeneous Assay
aSyn	Alpha-synuclein
BME	Beta-mercaptoethanol
Cryo-EM	Cryo-electron microscopy
EOPD	Early-onset Parkinson's Disease
FBS	Fetal bovine serum
FC	Flow cytometry
Fmax	Maximum fluorescence
FP	Fast-progressing
FRET	Fluorescence resonance energy transfer
HCI	High-Content Imaging
IFD	Integrated FRET Density
LagT	Lag time
LB	Lewy body
LBD	Lewy Body Dementia
LN	Lewy neurite
LOPD	Late-onset Parkinson's Disease
LP	Lewy-related pathology
NACP	Non-Abeta component of amyloid precursor protein
PBS	Phospate-buffered saline

✉ Pamela J. McLean
mclean.pamela@mayo.edu

[1] Department of Neuroscience, Mayo Clinic, 4500 San Pablo Road S, Jacksonville, FL 32224, USA

[2] Mayo Clinic Graduate School of Biomedical Sciences, Mayo Clinic, 200 First St. SW, Rochester, MN 55905, USA

PD	Parkinson's Disease
PFF	Pre-formed fibril
PK	Proteinase K
PMI	Post-mortem interval
PMSF	Phenylmethylsulfonyl fluoride
pSer129	Phosphorylated serine-129
pSer129-aSyn	Ser129-phosphorylated aSyn
PTM	Post-translational modification
RFU	Relative fluorescent unit
ROC	Receiver operating characteristic
RT-QuIC	Real-time quaking-induced conversion
SAA	Seed amplification assay
SD	Standard deviation
SDS	Sodium dodecyl sulfate
SP	Slow-progressing
T50	Time to reach 50% of the maximum fluorescence
TBS	Tris-buffered saline
ThT	Thioflavin T
WB	Western blotting

Introduction

Parkinson's disease (PD) affects over 10 million individuals globally and is one of the most prevalent neurodegenerative disorders. Clinically, PD is defined by hallmark motor symptoms—tremor, rigidity, akinesia/bradykinesia, and postural instability—as well as a broad spectrum of non-motor features that significantly contribute to disease burden and decreased quality of life [39, 52].

Neuropathologically, PD is characterized by the abnormal accumulation of misfolded alpha-synuclein (aSyn) within intraneuronal inclusions known as Lewy bodies (LBs) and Lewy neurites (LNs), collectively referred to as Lewy-related pathology (LP) [12, 21]. While aSyn aggregation is a defining feature of PD and related synucleinopathies, clinical manifestations vary widely among patients. Differences in age of onset, disease progression, and cognitive or neuropsychiatric involvement underscore heterogeneous disease trajectories [15, 60]. Understanding the molecular basis of this heterogeneity will be essential to elucidate PD pathogenesis and develop personalized therapeutic approaches.

Post-translational modifications (PTMs) of aSyn are believed to influence its aggregation, stability and toxicity [23]. Among these, phosphorylation at serine-129 (pSer129) is the most extensively studied. This modification is highly enriched in aSyn species found within Lewy pathology when compared to healthy brain tissue [17] and is widely used as a biomarker in experimental and neuropathological studies due to its strong association with intracellular aggregates. However, its precise role in disease pathogenesis remains unclear, necessitating further investigation into how pSer129 influences aggregation and contributes to clinical heterogeneity in PD.

A key mechanism driving disease progression is the prion-like behavior of misfolded aSyn where misfolded aSyn can propagate across cells and interconnected brain regions [24, 35]. Cell-free seed amplification assays (SAAs), including real-time quaking-induced conversion (RT-QuIC) and cell-based biosensor assays, offer sensitive tools for detecting aSyn seeding bioactivity and assessing conformational diversity or strain-like properties of aSyn aggregates [8, 61]. These assays provide a promising avenue for linking molecular diversity in aSyn to clinical variability in PD.

Emerging evidence suggests that distinct patient subgroups may harbor unique molecular profiles of aSyn pathology [30]. For instance, early-onset PD (EOPD), typically diagnosed before the age of 50, is often associated with genetic contributions and frequently exhibits slower progression [36, 44]. By contrast, late-onset PD (LOPD) is more closely associated with age-related cellular decline [3], while slow- and fast-progressing PD subgroups differ in clinical trajectory and treatment response [22, 51]. To date, the molecular underpinnings of disease heterogeneity remain poorly understood.

In this study, we asked whether molecular differences in aSyn are associated with clinical heterogeneity in PD. Using well-characterized postmortem brain tissue from clinically defined PD subgroups, we employed a multimodal approach integrating cell-based biosensor seeding assays, kinetic analyses of SAAs, quantification of total and phosphorylated αSyn levels, and proteinase K (PK) digestion profiling. By comparing EOPD and LOPD, as well as slow- and fast-progressing subgroups, we investigated subgroup-specific differences in aSyn aggregation and seeding potential. Our findings offer new insights into the molecular basis of PD heterogeneity which may inform the development of more targeted therapeutic strategies.

Materials and methods

Study cohort

Postmortem human brain samples from a clinically and neuropathologically well-characterized cohort were obtained from the Mayo Clinic Brain Bank, Jacksonville, Florida. A total of 63 individuals of European descent were included in the study, representing two distinct PD subtypes: early-onset (EOPD, onset < 60 years) and late-onset (LOPD, onset > 60 years). Within the LOPD group, patients were further stratified based on disease progression rate into slow-progressing (SP-LO, disease progression of more than 10 years), and fast-progressing (FP-LO, disease progression of less than 5 years) PD. A cohort of non-Lewy body

(non-LB) controls without synucleinopathy was included for comparison. All Lewy Body dementia (LBD) cases were clinically diagnosed with PD or Parkinson's disease dementia (PDD) and were neuropathologically confirmed to have LB disease. Metadata including age at onset, disease duration, progression rate (Fig. 1a-c) and APOE genotype were available for all samples (Table 1 and Supplementary Table 1). While all cases had confirmed neuropathological diagnosis and clinical diagnosis, more detailed clinical information was not available for every individual due to the donations of the post-mortem brains to the brain bank coming from multiple sources. One patient was excluded from the analysis due to a post-mortem interval (PMI) substantially longer than that of all other patients in the cohort, to minimize potential confounding effects on protein integrity and assay readouts.

Neuropathological assessment

A standardized neuropathologic evaluation was conducted for all cases by the same neuropathologist, including macroscopic observation, histologic assessment of hematoxylin and eosin-stained sections, fluorescent microscopy of thioflavin S (thioS) staining, and aSyn immunohistochemistry as

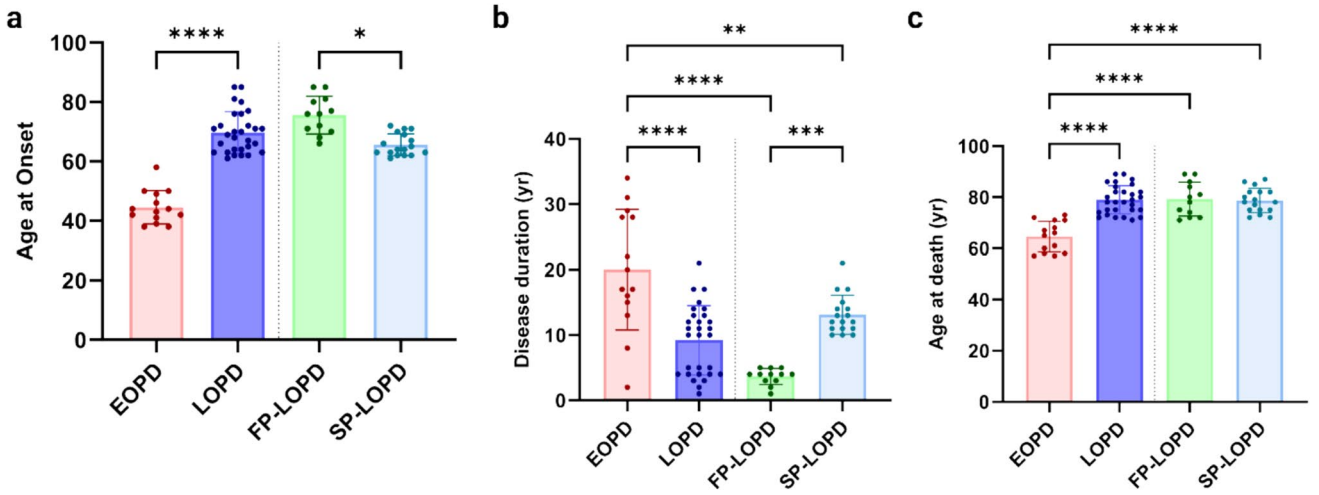

Fig. 1 Bar graphs with individual data points show (**a**) age at onset, (**b**) disease duration, and (**c**) age at death across early-onset PD (EOPD), late-onset PD (LOPD), fast-progressing late-onset PD (FP-LOPD), and slow-progressing late-onset PD (SP-LOPD) groups. Data are presented as mean ± SD with each dot representing an individual case. Statistical comparisons were performed using one-way ANOVA followed by Tukey's multiple comparison test for group comparisons

Table 1 Individual characteristics

PD Subgroup	Definition	*N*	Mean Age at Onset (years) (min–max)	Mean Disease Duration (years) (min–max)	Mean Age at Death (years) (min–max)	Sex (M/F)	Brainstem (BLBD) N (%)	LBD subtype Transitional (TLBD) N (%)	Diffuse (DLBD) N (%)
Early-onset PD (EOPD)	Onset < 60 years	14	44.6 (38—58)	20 (2—34)	64.6 (57—73)	12/2	1 (7.1%)	5 (35.7%)	8 (57.2)
Late-onset PD (LOPD)	Onset > 60 years	29	69.7 (61—85)	9.2 (1—21)	78.9 (71—89)	23/6	0 (0%)	13 (44.8%)	16 (55.2%)
Fast progressing (FP-LO)	Duration < 5 years	12	75.5 (66—85)	3.7 (1—5)	79.2 (71—89)	8/4	0 (0%)	4 (33.3%)	8 (66.7%)
Slow progressing (SP-LO)	Duration > 10 years	17	65.6 (61—72)	13.1 (10—21)	78.7 (72—87)	15/2	0 (0%)	9 (52.9%)	8 (47.1%)
Non-LB Controls	NA	20	NA	NA	70.3 (55—94)	10/10	NA	NA	NA

PD Parkinson's disease, *LB* Lewy body, *LBD* Lewy body disease, *N* Number of individuals, *M* Male, *F* Female, *NA* Not applicable, *min* minimum, *max* maximum

previously described [47]. Immunohistochemistry for aSyn was performed following formic acid pretreatment using a Dako Autostainer with NACP antibody (Mayo Clinic; rabbit polyclonal; 1:3000). The neuropathologic diagnosis of LBD was determined based on the detection of LBs within susceptible brain regions. LBD subtypes were subsequently classified into brainstem, transitional (limbic), and diffuse (neocortical) subtypes according to the extent and anatomical distribution of Lewy-related pathology (Table 1) [13]. LB quantification in the cingulate cortex was performed on NACP-immunostained sections. The cingulate gyrus was selected because it is a limbic cortical region that consistently exhibits aSyn pathology in PD and is functionally relevant to both motor integration and cognitive and neuropsychiatric manifestations of the disease. The microscopic field with the highest LB density was identified, and LBs were counted at × 20 magnification. For this assessment, only LBs with visible cell nuclei were counted while LNs were excluded from the analysis. Braak neurofibrillary tangle stage [6] and Thal amyloid phase [53] were determined using thioS fluorescence microscopy. Small vessel disease was assessed on hematoxylin and eosin-stained sections and considered present when arteriolosclerosis accompanied by microinfarcts, microbleeds, or white matter ischemic changes was identified [46].

Preparation of soluble and insoluble fractions from postmortem brain tissue

All postmortem brain tissues used in this study were dissected from the cingulate gyrus. For each patient sample, ~ 180 mg frozen tissue was cut into small pieces (~ 1 mm^3) using a sterilized scalpel on a cutting board cooled on ice. At a ratio of 1 g tissue to 3 mL homogenization buffer (50 mM Tris–HCl, pH 7.4, 750 mM NaCl, 5 mM EDTA, with cOmplete™, Mini, EDTA-free Protease Inhibitor Cocktail (Millipore Sigma) and Halt Phosphatase Inhibitor Single Use Cocktail (Thermo Scientific) to 1X), tissue was homogenized with two ceramic beads (2.8 mm, Omni International) using a bead homogenizer (VWR Mini Bead Mill) at speed 4 for 1 min. The homogenate was centrifuged at 85,000 × *g* for 20 min at 4 °C and the supernatant was collected as the "buffer-soluble" fraction. The pellet was subsequently re-homogenized in 1% Triton X-100 in homogenization buffer and centrifuged a second time at 85,000 × g for 20 min and the supernatant was collected as the "detergent-soluble" fraction. The pellet was extracted with 1 M sucrose and 1% Triton X-100 in homogenization buffer to remove myelin then washed twice with detergent-free tris-buffered saline (TBS) to minimize residual detergent carryover. The final pellet was resuspended in TBS with protease inhibitor, aliquoted, and frozen at −80 °C for use as the "detergent-insoluble" fraction.

AlphaLISA assay for total and phosphorylated serine 129 aSyn (pSer129-aSyn)

Amplified Luminescent Proximity Homogeneous Assay (AlphaLISA) is a highly sensitive, bead-based immunoassay that enables semi-quantitative and quantitative detection of target proteins in biological samples such as tissue or cell lysates using Alpha technology. AlphaLISA was used to measure total aSyn and phosphorylated Serine 129 aSyn (pSer129-aSyn) levels in detergent-insoluble fractions. Assays were performed using commercially available kits specific for total aSyn (Revvity, ALSU-TASYN-B-HV) and pSer129-aSyn (Revvity, ALSU-PASYN-B-HV) according to the manufacturer's instructions and protocols optimized for brain homogenates.

Detergent-insoluble brain fractions were prepared by standard detergent extraction protocols. For AlphaLISA, these fractions were diluted 2.5-fold with the kit-provided lysis buffer and incubated on ice for 20 min. For quantitative measurements, recombinant human aSyn (Proteos, RP-003) and recombinant human pSer129-aSyn (Proteos, RP-004) proteins were used to generate standard curves for total and pSer129-aSyn quantification, respectively. 15 µL of the diluted sample was added to each well of a low-volume HTRF 96-well plate (Revvity, 66PL96025). 7.5 µL of the AlphaLISA Acceptor Mix, prepared fresh using Reaction Buffer 1, Reaction Buffer 2, Activation Buffer, and Acceptor beads, was added to each well containing samples or standards. Plates were sealed with adhesive film, covered with foil to protect from light, and incubated at room temperature for 1 h. Subsequently, 7.5 µL of the Donor Mix, prepared using Dilution Buffer and Donor beads, was added to each well under low-light conditions. Plates were resealed and incubated for an additional 2 h at room temperature in the dark. AlphaLISA signal intensity was measured using an EnVision microplate reader (PerkinElmer, Waltham, MA) in Alpha Screen mode. The assay was performed with four replicates per sample across three repetitions for quantitative analysis and two repetitions per sample for semi-quantitative analysis.

Real-time quaking-induced conversion (RT-QuIC) assay

RT-QuIC is a highly sensitive and specific cell-free aSyn seed amplification assay (SAA) that detects minute amounts of seeding-competent aSyn species. RT-QuIC was performed to evaluate aSyn seeding activity in detergent-insoluble brain fractions. The reaction mixture contained 1X phosphate-buffered saline (KD Medical, PBS 10X, pH 8.0), 0.0006% sodium dodecyl sulfate (SDS), 10 µM Thioflavin T (ThT), and 0.1 mg/mL recombinant human aSyn monomer (Proteos, RP-010). Prior to use, the recombinant

aSyn was filtered using a 100 K cut-off centrifugal concentrator (Pierce, 88503) to remove potential aggregates and ensure monomeric protein input. Reactions were assembled in black 96-well plates with optical bottom (Nunc, 265301), preloaded with five or six low-binding silica beads (800 um, OPS Diagnostics, BLBG 800-200-03) per well. Detergent-insoluble brain fractions were diluted to 10^{-4} in PBS (KD Medical, Cat# RGF-3215, pH 8.0) and 5 ul was added to each well along with 95 ul of reaction mix. The plates were sealed and incubated in a FLUOstar Omega plate reader (BMG Labtech, Germany) at 42 °C, using cycles of 1-min double-orbital shaking followed by stationary incubation. ThT fluorescence was measured every 30 min at excitation/emission wavelengths of 450/480 nm over a total duration of 72 h. All RT-QuIC assays included positive and negative controls for background normalization: 0.001 mg/ml aSyn pre-formed fibrils (PFFs) and 1X PBS (KD Medical, pH 8.0), respectively. PFFs were generated in-house according to the Powers & Patel protocol [38].

After the assay, RT-QuIC plates were briefly centrifuged at 3000 rpm for 5 min to collect reaction products. Samples were then pooled per case, aliquoted and stored at −20 °C for a later PK assay.

Baseline correction was performed by averaging the fluorescence values from the first five readings for each well and subtracting this baseline from all subsequent measurements. The fluorescence threshold for a positive reaction was defined as the baseline plus five standard deviations (baseline + 5 SD) of the initial signal. A well was considered positive when the ThT fluorescence crossed this defined threshold. Each sample was tested in four technical replicates. Samples were classified as positive if three or four of the replicates crossed the fluorescence threshold. Samples with two positive replicates were considered inconclusive, and those with zero or one positive replicate were classified as negative. Seeding kinetics were analyzed by calculating the lag time (LagT), defined as the time required to reach the fluorescence threshold. Additional kinetic parameters, including time to maximum fluorescence (Time to Fmax) and T50 (time to reach 50% of the maximum fluorescence), were also calculated. LagT values were used for receiver operating characteristic (ROC) curve analysis to evaluate the diagnostic performance of the assay. Time to Fmax and T50 were only compared within PD subgroups, as most control samples did not reach the required fluorescence levels to assess these parameters.

Proteinase K (PK) assay and silver staining

10µL of SAA products were digested in 0.1 µg/µL PK in TBS + 0.1% SDS for 5, 30, and 60 min. To halt digestion and prepare samples for Silver Staining, the NuPage Sample Buffer and NuPage Reducing Agent (both Invitrogen) were added at 1X, and the samples were heated at 70 °C for 10 min.

Samples and 5 µl Precision Plus Protein Dual Color Standard (Bio-Rad) diluted 1:50 in water were loaded into NuPage 12% Bis–Tris gels (Invitrogen) and separated in ice-cold 1X MES SDS Running Buffer (Invitrogen) at 200 V for 55 min. Entire samples were loaded for the 5-, 30-, and 60-min time points, but only 25% of the undigested samples were loaded to avoid saturation.

PAGE gels were stained using the Pierce™ Silver Stain Kit (Thermo Fisher) according to the manufacturer's protocol and imaged using the pre-set Silver Stain program on the Bio-Rad ChemiDoc MP Imager. Using Bio-Rad Image Lab, the adjusted total band volumes representing signals from each timepoint were collected for analysis in Microsoft Excel and GraphPad Prism. Data are presented as a percentage of resistance: the total adjusted band pixel intensity at the 5-, 30-, 60-min timepoints were calculated as a percentage of the untreated 0-min timepoint.

Cell culture

The FRET biosensor cell reporter assay is a highly sensitive cell-based assay used to monitor and quantify intermolecular interactions of proteins, such as aSyn, particularly those linked to neurodegenerative diseases, such as PD [34]. HEK293T biosensor cell lines expressing both CFP-aSyn and YFP-aSyn (HEK.A53T-C/Y) (Dr. Marc Diamond, UT Southwestern) were used for high-content imaging (HCI) and Fluorescence Resonance Energy Transfer (FRET) assays. HEK293T wildtype (WT) cells (ATCC) and those expressing either CFP-aSyn only (HEK.A53T-CFP) or YFP-aSyn only (HEK.A53T-YFP) (Dr. Marc Diamond, UT Southwestern) were used for controls and gating in the FRET flow cytometry assay.

All cells were cultured in OptiMEM supplemented with GlutaMAX (Gibco) + 10% fetal bovine serum (FBS; Gibco) and maintained at 37 °C in a 5% CO_2 humidified incubator. Cells were routinely passaged for maintenance between 80 and 100% confluence, ~ 1–2 times per week as needed. Cells were tested for mycoplasma contamination at regular intervals.

Förster resonance energy transfer (FRET) assay

HEK.A53T-C/Y cells were plated in 24-well plates at 150,000 cells/mL and incubated for 24 h. Cells were treated with 25 µl of detergent-insoluble brain homogenate fractions, sonicated with Bioruptor Plus (Diagenode) at 10 °C for 10 cycles of 30 secs on, 30 secs off and incubated for 30 min with Lipofectamine 2000 (Invitrogen), for a further 48 h. As a positive FRET control, some cells were treated

with 0.1 mg/mL aSyn PFFs sonicated and prepared in the same way as the detergent-insoluble fraction-treated cells.

To prepare controls for the assay, WT HEK293 cells were transiently transfected with CFP or YFP (negative control) or CFP fused to YFP (positive control) using Lipofectamine 2000 (Invitrogen) for 48 h before flow cytometry (FC). HEK.A53T-CFP and HEK.A53T-YFP were used as additional negative controls to set the FC gates [18, 27].

To prepare samples and controls, individual wells were scraped and transferred in PBS to individual wells of a round-bottom 96-well plate. Following centrifugation, cells were stained with Zombie NIR Viability Dye (BioLegend, 1:300 dilution in PBS) for 30 min at room temperature. After incubation, cells were washed with PBS, fixed in 2% paraformaldehyde (PFA) for 15 min, and subsequently washed twice with FC buffer (PBS containing 2% FBS). Finally, cells were resuspended in the FC buffer for acquisition. Control samples were transferred to 1.5 mL tubes for setting gates and compensation, while treated samples remained in the 96-well plate for FRET acquisition.

Flow cytometry gating was established using the negative and positive cell line controls described above. WT HEK293T, HEK.A53T-CFP and HEK.A53T-YFP cells were used to define background fluorescence and set FRET-negative gates, while cells expressing CFP-YFP fusion were used to define the FRET-positive gate. A sequential gating strategy was applied uniformly. Events were first gated on forward scatter (FSC-A) versus side scatter (SSC-A) to exclude debris and identify the cell population. Gates were applied only to viable cells, as determined by Zombie NIR viability staining. Compensation for spectral spillover between CFP, YFP and FRET channels was performed using single-fluorophore control cell lines. To eliminate false-positive FRET arising from YFP bleed-through, a false-FRET gate was defined using YFP fluorophore cells. The final FRET-positive gate was established using negative control biosensor cells (CFP-YFP fusion cells) lacking seed material. Representative gating plots are provided in Supplementary Fig. 7. The FRET signal was quantified as Integrated FRET Density (IFD), calculated as the product of the percentage of FRET-positive viable cells and the median FRET intensity of those cells. This metric reflects both the extent and magnitude of aSyn seeding activity in each sample. Each sample was analyzed in five independent experiments, with three technical replicates per experiment. Technical replicates were averaged within each experiment to generate a single experimental value, and the final data point represents the mean of the five independent experiments for each sample.

High-content imaging (HCI)

To visualize and quantify intracellular aSyn aggregation, HEK.A53T-C/Y biosensor cells were imaged in the Operetta high-content imaging (HCI) system (Perkin Elmer). Cells were plated in black, clear-bottom 96-well plates (Celvis) at a density of 150,000 cells/mL 24 h before applying the same treatment protocols as in the FRET assay, again using 25 uL sonicated detergent-insoluble fractions. Following 48 h of incubation, cells were washed once with PBS and fixed with 4% PFA for 15 min at room temperature. After fixation, cells were washed with PBS and stained with Hoechst 33342 (#33342, Invitrogen; 1:10,000 dilution in PBS) for 5 min to visualize nuclei, followed by two additional PBS washes.

Images were acquired in the Hoechst, CFP, and YFP channels. Excitation of CFP and emission detection of YFP were used in a FRET-based configuration available on the imaging system to detect the presence of aSyn-aSyn interactions. Punctate aggregates were identified and quantified using Harmony image analysis software (PerkinElmer). The aggregate-to-nucleus ratio was calculated by normalizing the number of aSyn-positive aggregates to the number of Hoechst-stained nuclei per field. For each sample, 121 fields per well were analyzed across five replicates, ensuring robust and reproducible quantification of intracellular aggregate burden.

aSyn Immunodepletion from brain homogenates

To confirm the observed seeding activity was mediated by the aSyn in the brain homogenate we performed targeted immunodepletion on a randomly selected subset of brain homogenates. Protein G Dynabeads™ for immunoprecipitation (60 µL) (Invitrogen, # 10003D) were incubated with 10 µg/mL SYN211 antibody (anti–α-synuclein, Santa Cruz, # sc—12767) for 10 min at room temperature under gentle rotation. Following antibody coupling, the beads were immobilized on the magnetic rack, the supernatant was discarded, and the beads (conjugated and unconjugated) were washed once with 0.02% Tween-20 in PBS.

Brain homogenates were diluted 1:100 in PBS and sonicated for 10 min. Equal volumes of each sonicated homogenate were incubated either with SYN211-conjugated beads or with unconjugated beads for 15 min at room temperature with gentle rotation. After magnetic separation, the supernatants (depleted fractions) were collected and subjected to a second round of immunodepletion with SYN211-conjugated beads overnight at 4 °C. The depleted homogenates were collected, aliquoted, and stored at – 20 °C for WB and FRET seeding assays. Each sample was analyzed in three independent experiments for both WB and FRET assays and the values were normalized within each sample to its untreated baseline to assess relative depletion efficiency.

Western blotting (WB) of immunodepleted brain homogenates

Pierce BCA Protein Assay kit (23225; ThermoFisher) was used to determine total protein concentration in diluted or immunodepleted brain homogenates. 3 µg per sample was prepared for WB with 2X Laemmli loading buffer (Bio-Rad, #1610737), and 1:10 beta-mercaptoethanol (BME) (Bio-Rad, #1610710). Samples and the biotinylated ladder (Cell Signaling, #7727) were run on a Mini-PROTEAN TGX Stain-Free gel (Bio-Rad, #4568124) and transferred to a nitrocellulose membrane (Immobilon-P, Millipore). Membranes were blocked for 1 h at RT in 10% non-fat dried milk added TBS-T (500 mM NaCl, 20 mM Tris, 0.1% Tween 20, pH 7.4) solution, incubated overnight at 4 °C with HRP anti-α-Synuclein (4B12, Biolegend) then washed with TBS-T solution and incubated for 1 h at RT with secondary antibodies (anti-biotin HRP-linked antibody (7075P5, Cell Signaling) or anti-mouse HRP-conjugated antibody (Goat anti-mouse Ig, Human ads-HRP, #1010-05, Southern Biotech)). Proteins were detected using an enhanced chemiluminescent detection system (ECL, MilliporeSigma Immobilon, #WBKLS0500) and imaged by ChemiDoc MP Imaging System (Bio-Rad). aSyn bands were identified and quantified using Image Lab software (Bio-Rad, RRID:SCR_014210), including normalization to total protein from stain-free labeling.

Statistical analysis

All data were analyzed using Graph Pad Prism 9.0.0 software (San Diego, CA). Firstly, the normality of the data was assessed using the Shapiro–Wilk test. For data distributed normally, parametric tests were applied, including one-way ANOVA followed by Tukey's multiple comparison test for group comparisons and unpaired two-tailed Student's t-tests for pairwise comparisons. If data did not follow a normal distribution, non-parametric tests were used: the Kruskal–Wallis test followed by Dunn's multiple comparison test for group comparisons and the Mann–Whitney *U* test for pairwise comparisons. Correlations between seeding assay, biochemical measurements and LB counts were evaluated using two-tailed Spearman rank non-parametric correlations. The Spearman correlation coefficient r and the p value are indicated in the figures. Results are presented as mean ± standard deviation (SD) within a 95% confidence interval, and $p < 0.05$ values were considered statistically significant ($*p \leq 0.05$, $**p \leq 0.01$, $***p \leq 0.001$, $****p \leq 0.0001$). P values between 0.05 and 0.1 are indicated in the figures.

Results

pSer129-aSyn levels in PD brain samples

Because pSer129-aSyn is recognized as a marker of Lewy-related pathology, we first measured total aSyn and pSer129-aSyn levels in the Triton X-100-insoluble fractions of postmortem tissues. Biochemical analyses using AlphaLISA demonstrated that pSer129-aSyn levels were elevated across all PD subgroups compared to control samples (Fig. 2a and b). Although total aSyn levels did not differ significantly between patient and control samples (Fig. 2a), subgroup analysis showed that LOPD had significantly higher total aSyn levels than both EOPD and controls (Fig. 2c) whereas pSer129-aSyn levels did not significantly differ between patient subgroups (Fig. 2d). Further stratification of LOPD patients into slow- and fast-progressing (SP-LO and FP-LO, respectively) disease groups did not reveal significant differences in total (Fig. 2e) or phosphorylated aSyn levels (Fig. 2f).

aSyn seeding activity in biosensor cells

To investigate seeding bioactivity of PD patient samples, the FRET-based biosensor cell line expressing aSyn-YFP/CFP fusion proteins was treated with Triton X-100-insoluble fractions of brain homogenates. As expected, all PD samples exhibited significantly higher seeding activity compared to controls with the FRET flow cytometry assay (Fig. 3a). Interestingly, substantial inter-individual variability in seeding potential was observed, with a more than tenfold difference observed across cases. This variability appeared to be driven primarily by individual patient differences rather than by subgroup classifications.

Subgroup analysis revealed no significant difference in seeding activity between EOPD and LOPD; however, LOPD patients exhibited significantly higher seeding activity compared to controls (Fig. 3b). Within the progression subgroups, SP-LO demonstrated higher seeding activity than FP-LO, although this difference was again mostly driven by individual variability (Fig. 3c and Supplementary Fig. 1).

Importantly, FRET signal intensity is positively correlated with pSer129-aSyn levels, indicating that phosphorylation at Ser129 is consistent with the formation or stabilization of seeding-competent aSyn species (Fig. 3d). Notably, two of three patients with the highest FRET signal and pS129-aSyn levels (highlighted in Fig. 3d) carried the E3/E4 genotype, suggesting that APOE4 could influence seeding activity in PD (Table 2 and Supplementary Table 1).

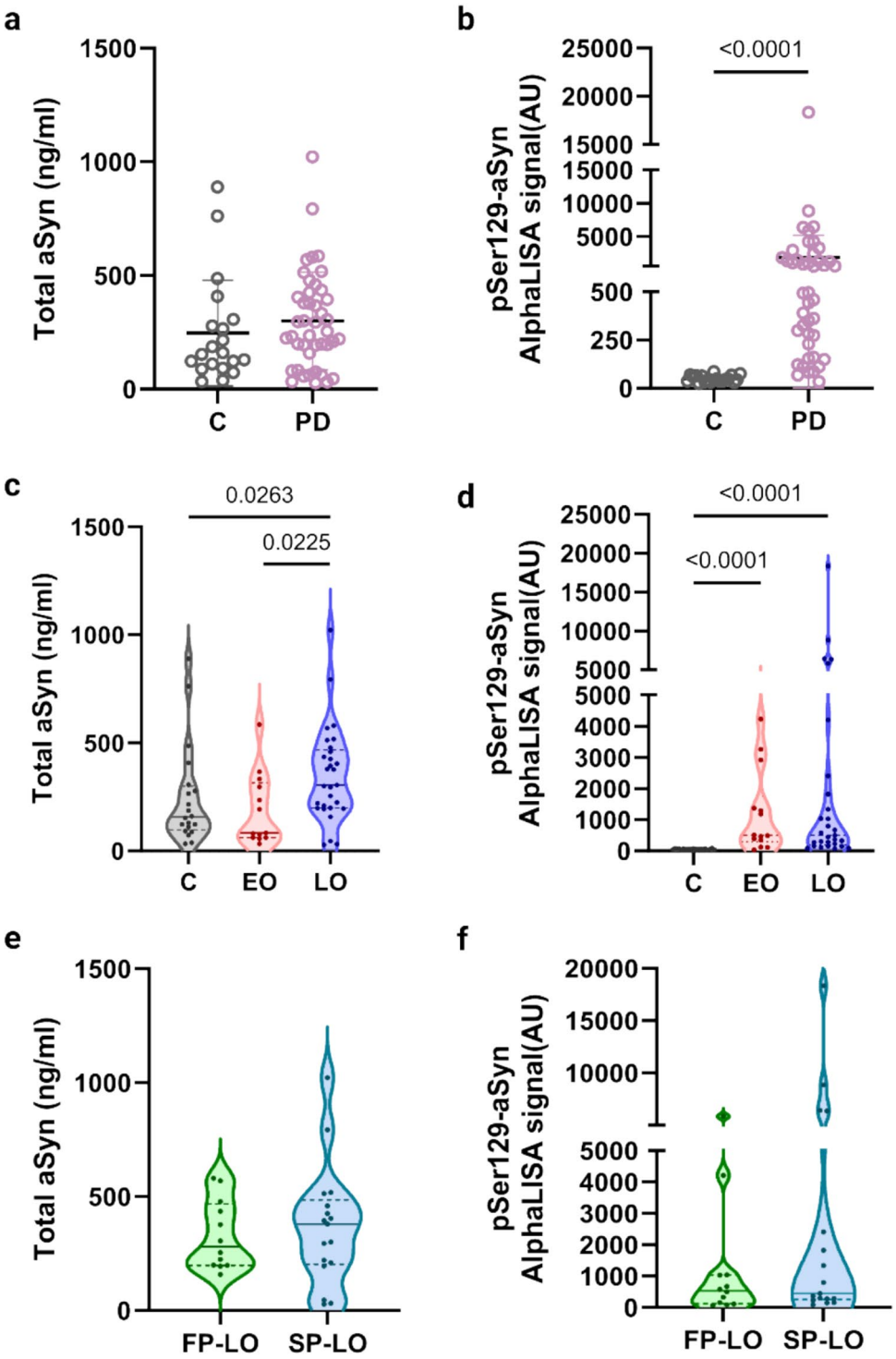

Fig. 2 Measurement of total and pSer129-aSyn levels in detergent-insoluble brain fractions by AlphaLISA. (**a** and **b**) total and pSer129-aSyn levels in PD and control (C) groups. (**c** and **d**) total and pSer129-aSyn levels across controls, EOPD and LOPD. (**e** and **f**) Comparison of total and pSer129-aSyn levels in FP-LO and SP-LO. Data represent mean ± SD. Each dot represents the average value for an individual case. Violin plots show the distribution of the data, with the median indicated by the central line and quartiles by the dashed lines. Statistical significance was determined using Kruskal–Wallis test followed by Dunn's multiple comparison test for group comparisons (c and d) and the Mann–Whitney U test for pairwise comparisons (a, b, c and e), and Student's t-test (f)

To determine whether the observed differences in FRET signal were related to cytotoxicity, a viability dye was multiplexed during flow cytometry; no significant differences in cell viability were detected across disease subgroups, confirming that the differences in FRET signal are not driven by acute cytotoxic effects (Fig. 3e).

aSyn immunodepletion reduces seeding activity in biosensor cells

To confirm that the observed seeding activity was mediated by aSyn, aSyn was immunodepleted from brain homogenates using protein G tagged Dynabeads conjugated with an anti-aSyn antibody. WB analysis confirmed

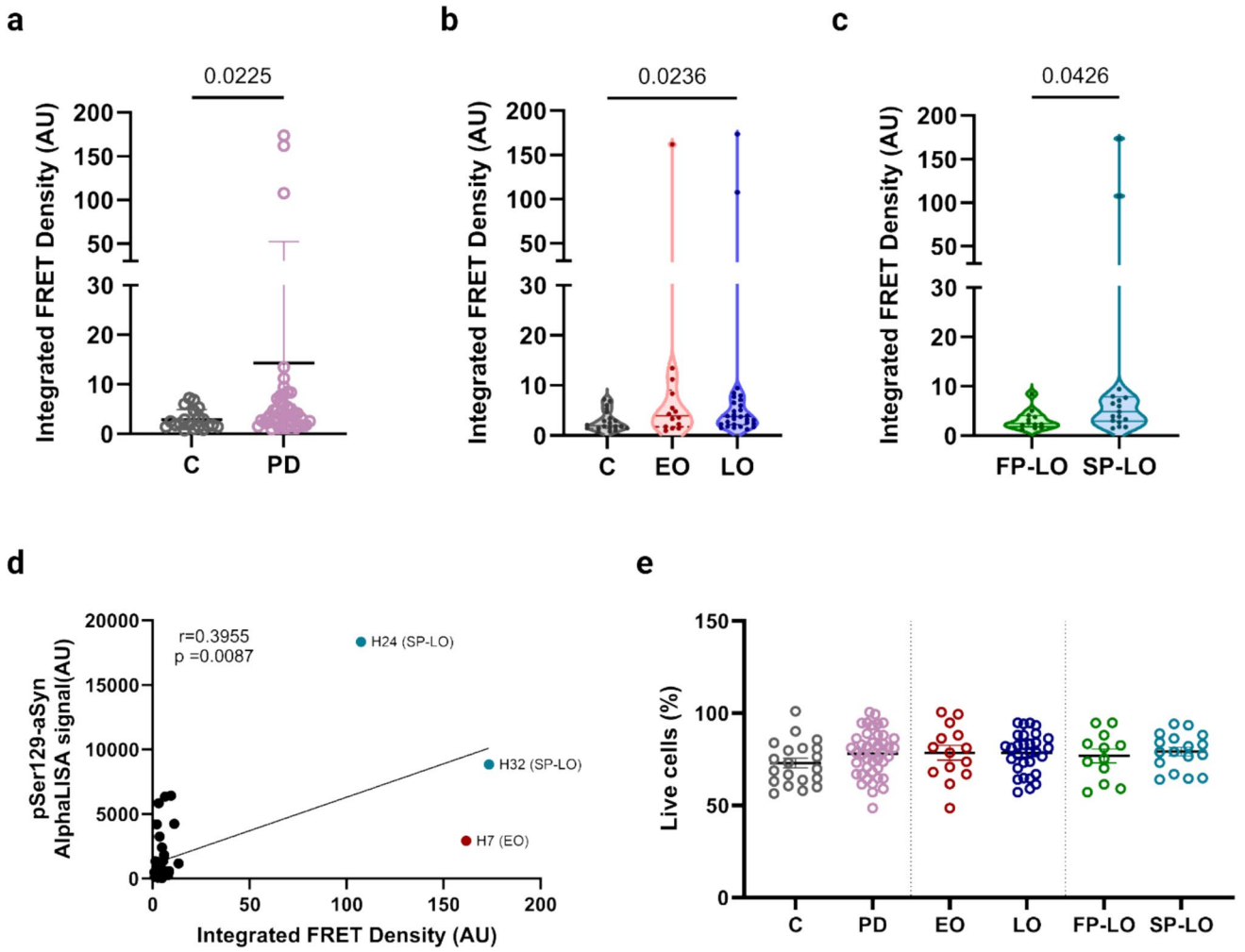

Fig. 3 aSyn seeding bioactivity measured by FRET FC assay. (**a**) Comparison of aSyn seeding activity in PD and control (C) groups. (**b**) Comparison of aSyn seeding activity in EOPD and LOPD disease subgroups. (**c**) Comparison of aSyn seeding activity in FP-LO and SP-LO subgroups. (**d**) Correlation between pSer129-aSyn levels and FRET seeding bioactivity in PD cases. (**e**) Cell viability analysis following treatment with detergent-insoluble brain fractions. Data represent mean ± SD. Each dot represents the average value for an individual case. Violin plots show the distribution of the data, with the median indicated by the central line and quartiles by the dashed lines. Statistical significance was determined using Kruskal–Wallis test followed by Dunn's multiple comparison test for group comparisons and the Mann–Whitney U test for pairwise comparisons. For the correlation analysis, a two-tailed Spearman's rank correlation test was used, and r and p values are indicated on the plot

an average depletion of 64% in aSyn levels relative to untreated homogenates (Supplementary Fig. 2).

Seeding potential was assessed using the FRET-FC assay as previously described. Consistent with the partial depletion of aSyn species, immunodepleted samples had an average reduction of 71% in integrated FRET intensity relative to untreated samples (Supplementary Fig. 2) indicating a decrease in seeding bioactivity and confirming a contribution of aSYN to the observed seeding.

Intracellular aggregate burden quantified by high content imaging

Using the same FRET biosensor cell model, we performed imaging to further observe the intracellular burden of aSyn aggregates. Aggregate load was quantified by calculating the aggregate-to-nucleus ratio, providing an independent burden measure of seeding bioactivity.

Table 2 ApoE profiles of individuals

PD Subgroup	N	ApoE ε2/ε3 N (%)	ApoE ε3/ ε3 N (%)	ApoE ε3/ ε4 N (%)	ApoE ε4/ ε4 N (%)
Early-onset PD (EOPD)	14	1 (7.1%)	7 (50)	6 (42.9%)	0 (0%)
Late-onset PD (LOPD)	29	1 (3.4%)	18 (62.1%)	10 (34.5%)	0 (0%)
Fast progressing (FP-LO)	12	0 (0%)	6 (50%)	5 (41.7%)	1 (8.3%)
Slow progressing (SP-LO)	17	1 (5.9%)	12 (70.6%)	4 (23.5%)	0 (0%)

PD Parkinson's disease, *ApoE* Apolipoprotein E, *N* Number of individuals

Consistent with FRET-based flow cytometry, all PD samples induced significantly greater intracellular aggregate formation compared to controls (Fig. 4a and b). Subgroup analysis revealed no significant differences in aggregate burden between EOPD and LOPD patients; however, the LOPD group had significantly higher aggregate counts than controls (Fig. 4a and c). Additionally, SP-LO demonstrated a greater intracellular aggregate burden compared to FP-LO patients (Fig. 4c and d).

Seeding activity and kinetics measured by aSyn-SAA

To validate and extend the cellular seeding results, the same detergent-insoluble fractions were subjected to SAA. Each sample was analyzed in quadruplicate. Samples were classified as positive if three or four of the replicates crossed the calculated fluorescence threshold. Samples with two positive replicates were considered inconclusive, and those with zero or one positive replicate were classified as negative (Fig. 5a). Individual curves display the mean relative fluorescent unit (RFU) values across quadruplicate reactions for each sample (Supplementary Fig. 3).

All PD samples were positive (4/4 replicates), demonstrating robust and consistent seeding activity. Among control samples, 15 were negative, 3 were inconclusive, and 2 controls exhibited positive seeding with 3/4 replicates.

Seeding kinetics were calculated using lag time (LagT), time to maximum fluorescence (Time to Fmax), and T50 (time to half-maximal fluorescence). LagT analysis revealed that PD had significantly shorter mean lag times (26.9 h) compared to controls (45.1 h) to reach the threshold, indicating faster aggregation initiation in PD samples (Fig. 5b). ROC analysis of lagT demonstrated an area under the curve (AUC) of 0.98 with the optimal lag time cutoff of < 34.7 h achieving 93% sensitivity and 100% specificity, supporting lag time as a highly reliable discriminator between PD and control brain samples. Time to Fmax and T50 were only analyzed within PD subgroups, as most control samples did not reach minimum fluorescence levels for these measurements. No statistically significant differences were detected between patient groups (Fig. 5c and d).

Proteinase K digestion indicates conformational heterogeneity of aSyn aggregates

We performed PK digestion on SAA-amplified aSyn products to investigate potential differences in proteolytic resistance, which may be indicative of conformational differences. In the absence of PK, a single aSyn band was observed at the expected size (~ 15 kDa) of the aSyn monomer under denaturing conditions that was comparable across samples. Following PK treatment, amplified products exhibited differential resistance profiles. Banding patterns of PK-digested samples revealed a consistent pattern across PD subgroups, with comparable fragment sizes and distribution of protease-resistant bands and a protease-resistant core between groups. Representative PK digestion profiles are shown in Fig. 6a, and full membrane images for all samples are provided in Supplementary Fig. 6. PD patient samples were more resistant to digestion at all time points, compared to non-LB controls (Fig. 6b). Nevertheless, both PD and control samples were digested significantly compared to their starting time point conditions (Fig. 6b). While PD samples demonstrated increased resistance compared to controls, PK resistance did not significantly differ across patient subgroups defined by disease onset (Fig. 6c). When stratified by disease progression, a trend toward higher PK resistance was observed in FP-LO patients compared to SP-LO patients (Fig. 6d).

These findings suggest that seeding-competent species amplified during RT-QuIC exhibit differential proteolytic stability, with PD samples demonstrating greater resistance than controls. The variability observed at the individual sample level suggests conformational heterogeneity of amplified aSyn species rather than subgroup-specific structural distinctions. Such interindividual differences in PK resistance may reflect molecular diversity in aSyn aggregate structure across cases.

Association between seeding activity and Lewy pathology burden

To explore the relationship between biochemical measurements and neuropathological burden, LB counts were quantified in the cingulate gyrus (Fig. 7a-c). Representative immunohistochemical staining with the anti-NACP antibody illustrates differences in LBs between an exceptional case (Fig. 7d) and a typical PD case (Fig. 7e). LB quantification revealed no significant differences in LB counts between clinical PD subgroups (Fig. 7f). However,

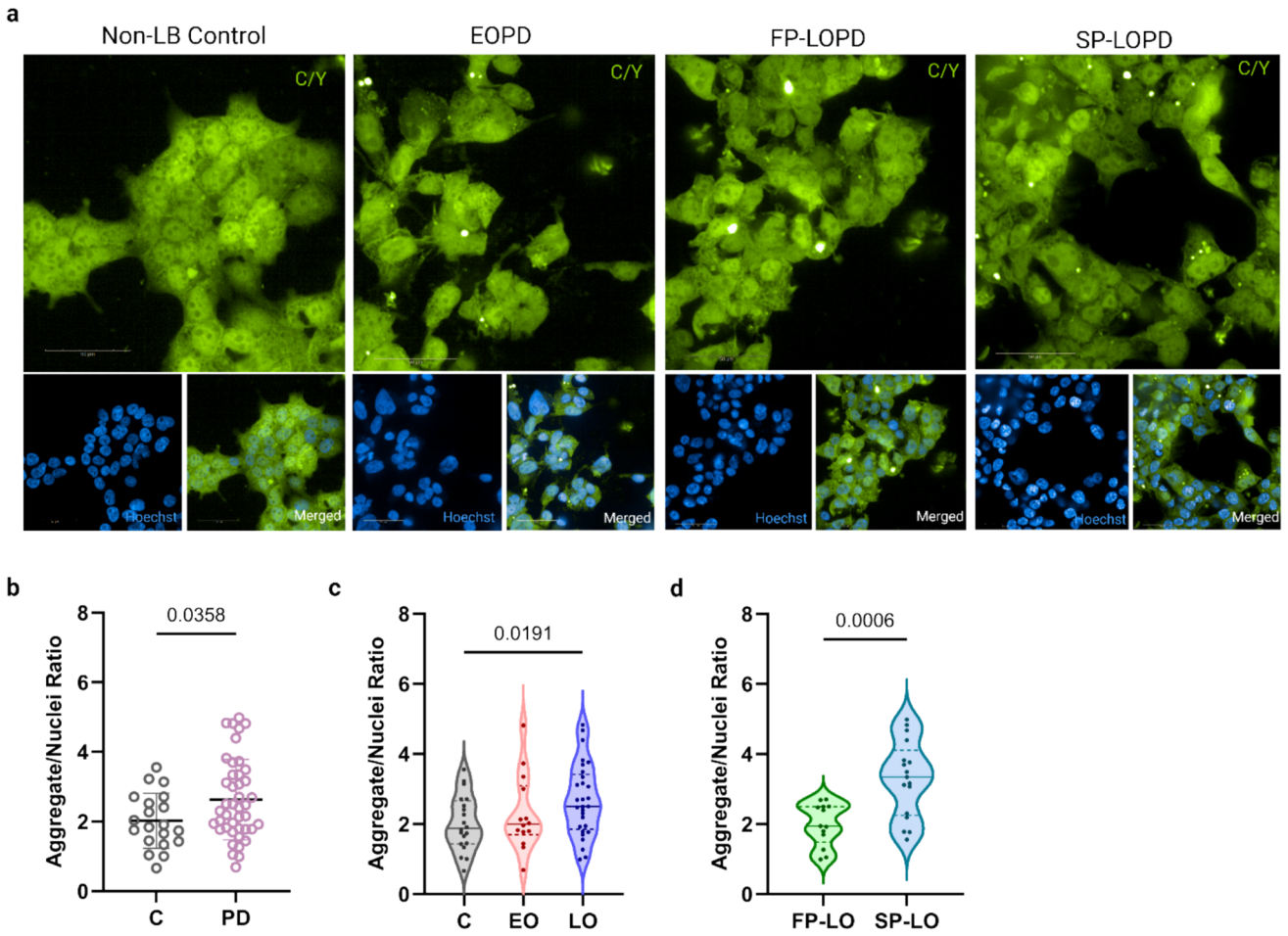

Fig. 4 Intracellular aSyn aggregates in biosensor cells. (**a**) HEK. A53T-C/Y cells were treated with detergent-insoluble brain fractions and imaged under conditions in which excitation was applied at CFP and emission was detected at YFP wavelengths, enabling FRET-based visualization of intracellular aggregate formation. The scale bar represents 50 µm. (**b**) Quantification of intracellular aggregates in PD and control (C) samples. (**c**) Quantification of intracellular aggregates across controls, EOPD and LOPD. (**d**) Within LOPD subgroups, comparison of aggregate burden in FP-LO and SP-LO patients. Data represent mean ± SD. Each dot represents the average value for an individual case. Violin plots show the distribution of the data, with the median indicated by the central line and quartiles by the dashed lines. Data are shown as violin plots normalized to the negative control condition (lipofectamine-treated cells set to 1). Statistical analysis was performed using one-way ANOVA followed by Tukey's multiple comparison test for group comparisons and unpaired two-tailed Student's t-tests for pairwise comparisons

LB counts positively correlated with pSer129-aSyn levels and FRET signal intensity (Fig. 7g), indicating that higher seeding activity and pSer129-aSyn levels are associated with increased LB pathology.

Discussion

In this study, we applied an integrated, multimodal biochemical and cell-based approach to investigate the molecular diversity of aSyn across clinically and pathologically defined PD subgroups. By combining the cell-based biosensor reporter assay and cell-free seed amplification assays (SAAs), protein-level measurements, and PK digestion profiling, we identified inter-individual differences in aSyn aggregation and seeding potential. Our findings highlight that pSer129-aSyn is strongly associated with both aggregation burden and seeding bioactivity, supporting its role as a key molecular correlate of PD.

Consistent with prior reports [2, 17, 55], we observed elevated pSer129-aSyn levels in PD compared to controls, confirming its utility as a robust pathological marker of synucleinopathy. Interestingly, while total aSyn levels were not significantly different across PD subgroups, LOPD cases showed higher total aSyn levels compared to both EOPD and controls. This may suggest that the increased aSyn burden contributes more prominently to pathogenesis in LOPD, in contrast to EOPD where other molecular factors

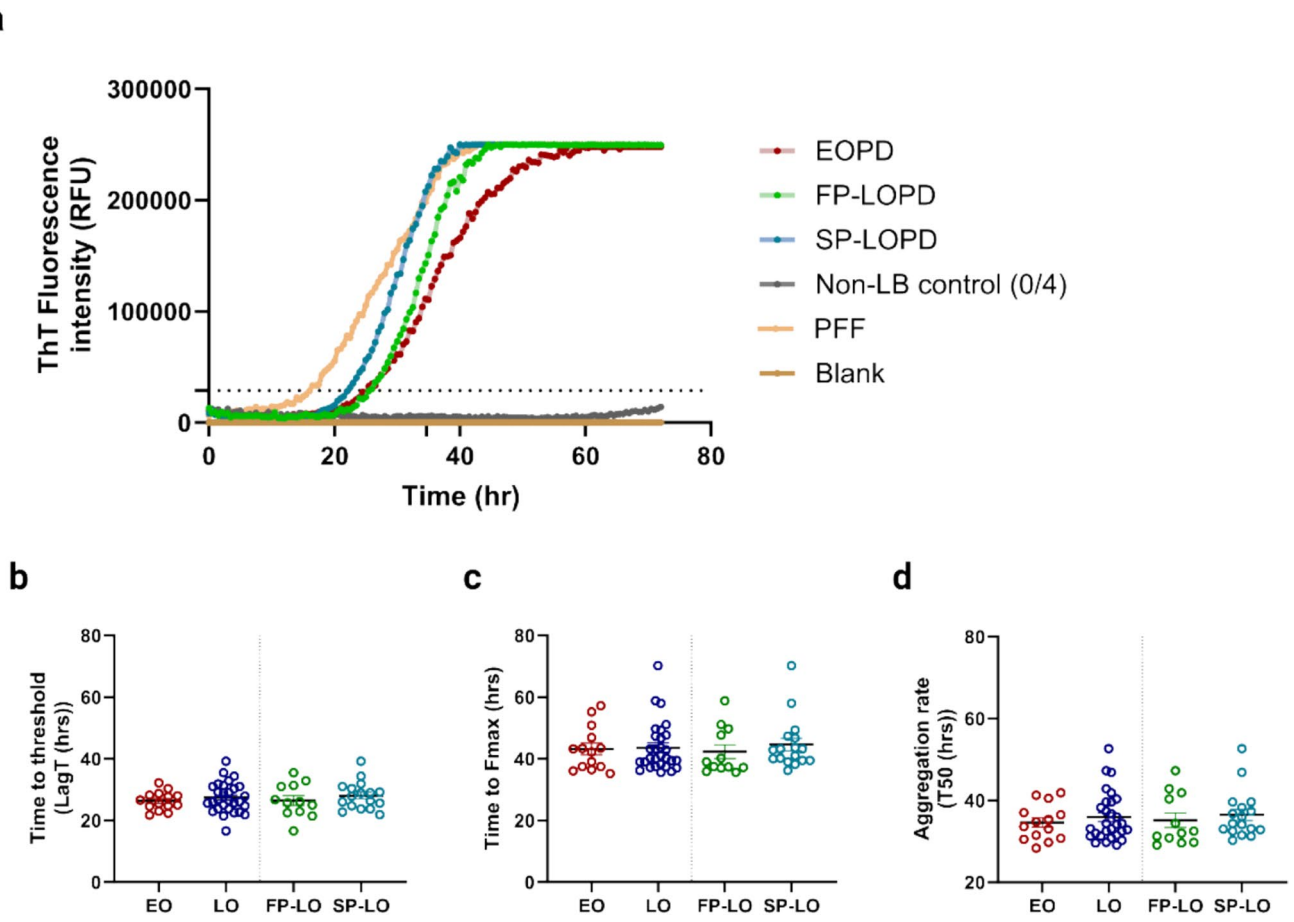

Fig. 5 RT-QuIC of detergent-insoluble brain fractions. (**a**) Representative ThT fluorescence traces for an individual from each group. Curves show the mean RFU values of quadruplicate wells for each case. (**b**) LagT analysis showed significantly shorter lag times in PD compared to controls. However, no differences were detected in PD patient subgroups. (**c**) Time to Fmax analysis in EO, LO, FP-LO and SP-LO groups. (**d**) T50 analysis in EO, LO, FP-LO and SP-LO groups. Statistical analyses: Student's t test was used for LagT analysis, and Mann–Whitney U test was used for Time to Fmax and T50 analyses. RFU: Relative fluorescent unit

(e.g., genetic variants, mitochondrial dysfunction) may play greater roles [29, 45].

While pSer129-aSyn is strongly associated with and is a classic marker for LB pathology [33, 41], recent studies indicate that activity-driven phosphorylation of aSyn at S129 occurs under physiological conditions in response to neuronal activity, is reversible, and appears to regulate synaptic function without toxicity [37, 42]. Moreover, emerging evidence suggests that S129 phosphorylation may occur after aggregation rather than being an initiating event, with studies demonstrating that it can even inhibit further fibrillization [20]. Taken together, these findings suggest that although pSer129-aSyn accumulation is a defining feature of PD pathology, it may also act as a compensatory or modulatory mechanism within the disease progress. The correlation we observed between pS129-aSyn and seeding indicates that phosphorylation may serve a dual role: reflecting aggregation load while also modulating the stability and propagation of pathogenic species. Our results reinforce the idea that pS129 is not just a bystander of pathology, but may be associated with aggregation dynamics in PD.

In biosensor-based seeding assays, even modest differences in aggregate counts are considered biologically meaningful because they reflect early templating efficiency and seeding competence [1, 32]. We observed significantly higher seeding activity in all PD subgroups compared with controls, accompanied by inter-individual variability that exceeded group-level differences. This is consistent with previous reports demonstrating that seeding activity is a sensitive marker of pathological aSyn species, but varies across individuals [49, 59, 61]. The positive correlation between FRET and pS129–aSyn levels further suggests that seeding activity is modulated by post-translational modifications. In Alzheimer's disease, patient-to-patient heterogeneity in tau biochemical and seeding properties has been shown to correlate with clinical aggressiveness [14]. In that study the authors found striking diversity in seed-competent tau species across individuals, with differences in post-translational

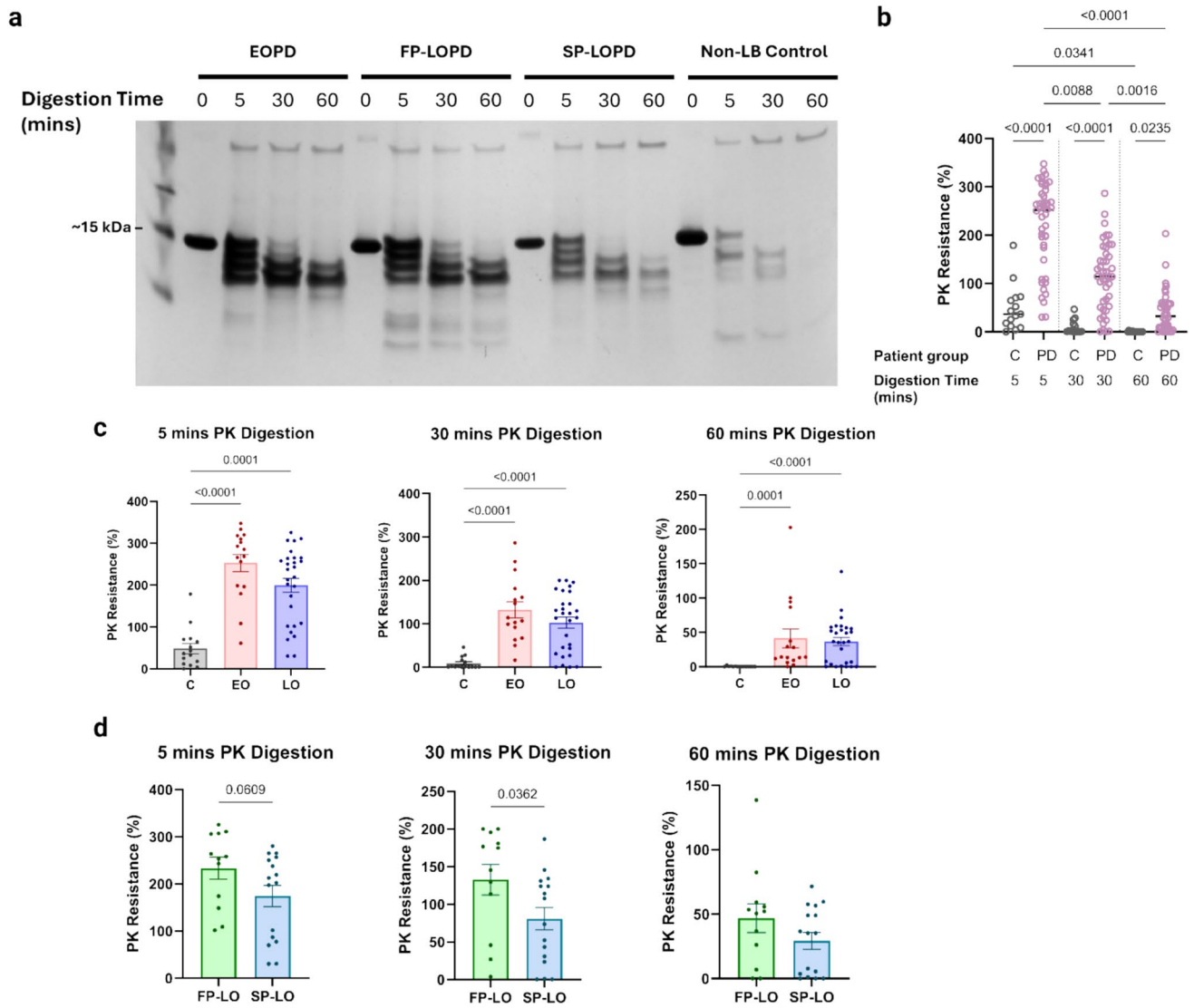

Fig. 6 Proteinase K (PK) digestion of seed amplification assay products identified differential proteolytic resistance profiles between controls (C) and PD patients. (**a**) Undigested product is shown on a Silver Stain at the expected band size for aSyn monomer (~15 kDa). PK digestion broke this product down over time. (**b**) PD patient products were more resistant than controls at all time points. (**c**) Although patient groups remained more resistant than controls, no differences within patient sub-groups were found in relation to disease onset. (**d**) Between late-onset patients, a trend toward higher resistance was observed in FP-LO patients. Data represent mean ± SD. Statistical significance was determined using Kruskal–Wallis test followed by Dunn's multiple comparison test for group comparisons and the Mann–Whitney U test for pairwise comparisons

modification patterns and aggregation kinetics that predicted rate of cognitive decline. Our data show a similar pattern: inter-individual variability in seeding bioactivity, linked to a post-translational modification (phosphorylation), that supports the idea that conformational diversity of aggregation-prone proteins may contribute to clinical heterogeneity across neurodegenerative disorders.

We performed a PK digestion assay on RT-QuIC-amplified end-products to enable biochemical characterization of seed competent aSyn species under standardized conditions. SAAs have been used for ultrasensitive detection of pathogenic seeds in cerebrospinal fluid [5], brain homogenates [54, 58], and peripheral tissues [11, 19]. Amplified SAA fibrils are commonly used to model intrinsic properties of the original seed competent species and have enabled the identification of disease-specific biochemical and structural differences across synucleinopathies [16, 50, 54].

Although previous studies have shown that SAA-derived fibrils can exhibit different structures from brain-derived aggregates, and end-products of amplification may not fully reflect the properties of the original material [31], a recent study demonstrated that amplified aSyn fibrils can retain

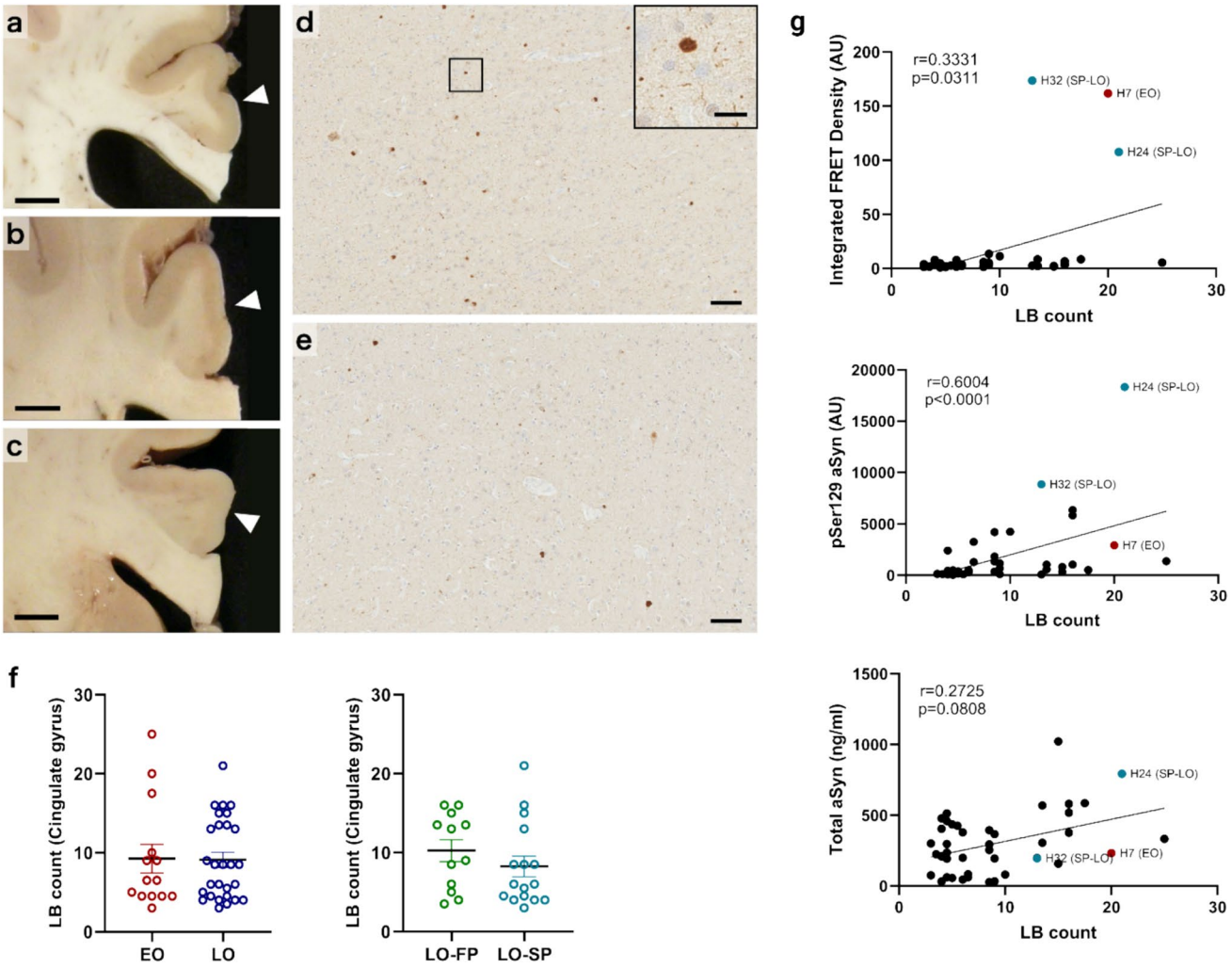

Fig. 7 Gross pathology of the cingulate gyrus and correlations with Lewy body (LB) burden and biochemical measures. Representative coronal brain sections of the cingulate gyrus showing the cingulate cortex (white arrowheads) in an exceptional case (**a**), a typical case (**b**), and a non-LB control (**c**). Gross examination shows cortical atrophy and pallor of the cingulate region in PD cases compared to controls. (**d and e**) Immunohistochemistry with anti-NACP antibody in the cingulate cortex; (a) and (d) are from the same patient, and (b) and (e) are from the same patient. Inset in (d) shows an LB at higher magnification. Scale bars: 5 mm (a–c); 100 µm (d and e); 20 µm (inset). (**f**) Quantitative analysis of LB counts across PD patients did not reveal significant differences between clinical subgroups, although substantial variability was observed within each group. (**g**) Spearman correlation analyses show a positive association between LB counts and integrated FRET density, pSer129-aSyn, and total aSyn levels in PD cases

key biological and structural features of the brain-derived strains. These amplified fibrils have been shown to exhibit comparable pathogenic activity in cellular models and to have similar protofilament conformations as determined by cryo-EM [56]. Further studies integrating biochemical, structural, and functional approaches will be important to better define specific aSyn strains or species to understand how these conformations contribute to aSyn aggregation.

Direct PK digestion of brain homogenates can fail to yield robust or reproducible banding patterns, likely due to the low amount of fibrillar aSyn in tissue extracts [31], whereas in vitro amplified material permits more consistent biochemical assessment. Consistent with these observations, we performed PK digestion on brain homogenates and failed to produce consistent PK-resistant bands, supporting our rationale for analyzing RT-QuIC end products. Accordingly, the PK digestion profiles are considered within a broader multimodal framework herein, and our conclusions regarding molecular heterogeneity are based on the combined interpretation of all experimental readouts.

Notably, differences in FRET signal were not accompanied by changes in cell viability across study groups. This finding is not unexpected, as biosensor-based seeding assays are designed to capture early aggregation and templating events that precede overt cytotoxicity. The lack of cytotoxicity indicates that the increased FRET signal

in PD patients compared to controls is unlikely to be confounded by nonspecific toxicity or cellular stress and instead reflects actual differences in aSyn seeding competence. Similar observations showing that aSyn seeding activity can occur independent of acute cytotoxicity have been reported in prior studies, supporting the interpretation that seeding competence and toxicity are not necessarily coupled at early stages of pathology [4, 7].

Indeed, neuropathological LB counts in the cingulate gyrus further supported these findings. LB counts were correlated with both pS129-aSyn levels and FRET seeding activity. This suggests that biochemical measures of aSyn pathology correlate with neuropathological burden. Importantly, these correlations indicate that seeding assays and phosphorylation markers capture aspects of disease biology beyond LBs, reflecting the dynamic aggregation potential of α-Syn. Such findings are consistent with prior reports emphasizing that soluble, oligomeric, and seeding-competent species may be more directly implicated in neurotoxicity and severity of the disease [46, 48] than bona fide LB pathology.

Clinical review of the three outlier patient samples did not reveal any atypical disease phenotypes. All three patients were reported to have a typical PD course characterized by motor symptom onset followed by gradual cognitive decline and eventually dementia. However, these cases exhibited features consistent with advanced diffuse cortical LB pathology and long disease duration, factors that may influence aSyn aggregate maturation, PTMs, and seeding behavior. Therefore, the observed molecular differences are more likely to reflect biological heterogeneity in aSyn pathology rather than distinct clinical phenotypes.

APOE ε4 allele is the strongest known genetic risk factor for Alzheimer disease (AD) and is also recognized as an important contributor to synucleinopathies, including PD and dementia with Lewy bodies (DLB) [62]. Emerging evidence indicates that APOE genotype has an impact on aSyn pathology, with APOE4 exacerbating aggregation, enhancing seeding activity, and promoting neurotoxicity [10, 62]. Furthermore, APOE4 has been shown to increase aSyn seeding activity and contribute to neurodegeneration in AD cases with LB pathology, underscoring its impact on mixed pathologies in the aging brain [28].

In our study, two of three patients with the highest FRET signal and pS129-aSyn levels (outlier 3 patients; H7, H32, and H24 (E3/E3)) carried the E3/E4 genotype, suggesting that while APOE4 may influence both aggregation burden and seeding activity in PD, it is not necessarily responsible. Interestingly, the ε4 allele was more frequent in FP-LO (50%) compared to SP-LO (23.5%) (Table 2). This distribution is consistent with previous reports associating APOE4 with more aggressive disease courses [40, 57], particularly in LOPD. Together, these findings point toward an association of APOE4 with molecular heterogeneity in PD.

Recent efforts to redefine synucleinopathies using biologically grounded frameworks, such as Neuronal alpha Synuclein Disease Integrated Staging System (NSD-ISS) and SynNeurGe, emphasize molecular characteristics of pathogenic aSyn in disease models rather than clinical classification alone [9, 43]. The SynNeurGe framework proposes a biologically based classification that integrates synucleinopathy, neurodegeneration, genetic risk, and clinical status to capture etiologic and phenotypic heterogeneity across the disease spectrum [25]. On the other hand, the NSD-ISS introduces a more restrictive biological definition centered on neuronal aSyn pathology, dopaminergic dysfunction, and specific genetic anchors [26, 43]. Although the present study does not formally classify cases within these frameworks, the inter-individual variability we observe in aSyn seeding activity, aggregation burden, and pSer129-aSyn levels is conceptually aligned with the core principles of both models. Our findings support the notion that molecular properties of pathogenic aSyn provide meaningful information beyond traditional clinical subgrouping based on age of onset or disease progression. In this context, molecular profiling approaches may contribute to the refinement and validation of emerging biological classification systems for PD.

In summary, this study suggests that aSyn pathology in PD is characterized by measurable differences in biochemical properties, aggregation burden, and seeding activity compared to controls, along with substantial variability between individuals. Across multiple complementary assays, this heterogeneity was not fully captured by clinical subgroup classifications based on age of onset or disease progression. While pSer129-aSyn levels, aggregation burden, and seeding activity were correlated, these relationships reflect associations rather than direct mechanistic links. These findings suggest that molecular variability in aSyn represents an important dimension of disease biology beyond current clinical stratification approaches and may help explain differences in disease trajectory and treatment response. This molecular heterogeneity highlights why a one-size-fits-all approach to therapy is unlikely to suffice, as distinct molecular profiles can underlie different disease trajectories and responses to intervention and may help inform the development of more targeted and individualized therapeutic strategies. Future studies in larger, well-characterized cohorts are required to determine whether these molecular features can be linked to clinical trajectories or used to inform biologically based classification frameworks.

Supplementary Information The online version contains supplementary material available at https://doi.org/10.1007/s00401-026-03026-1.

Author contributions Z.B.K contributed to conception, design, data acquisition, analysis, interpretation, and drafted the manuscript; D.A., A.S., M.J.L., M.B. and M.D. contributed to data acquisition; H.S. contributed to data acquisition and manuscript draft; S.L.B. contributed to analysis and interpretation; O.A.R. and D.W.D. contributed to data acquisition and interpretation; P.J.M. contributed to conception, design, and interpretation, and critically revised the manuscript. All authors proofread and approved the manuscript.

Funding This study was supported by the National Institute of Neurological Disorders and Stroke (NINDS) Lewy Body Dementia Center Without Walls (CWOW) Award (U54NS110435) (PJM, OAR, DWD), American Brain Foundation Cure One Cure Many Award (OAR, PJM), Ted Turner and family (OAR, PJM), and National Institute of Aging (NIA) R01AG087165 (OAR).

The content is solely the responsibility of the authors and does not necessarily represent the official views of the National Institutes of Health.

Data availability All data supporting the findings of this study are available within the paper and its Supplementary Information.

Declarations

Conflict of interests The authors declare no competing interests.

References

1. Algar WR, Hildebrandt N, Vogel SS, Medintz IL (2019) FRET as a biomolecular research tool — understanding its potential while avoiding pitfalls. Nat Methods 16:815–829. https://doi.org/10.1038/s41592-019-0530-8
2. Anderson JP, Walker DE, Goldstein JM, de Laat R, Banducci K, Caccavello RJ et al (2006) Phosphorylation of Ser-129 Is the Dominant Pathological Modification of & #x3b1;-Synuclein in Familial and Sporadic Lewy Body Disease *. J Biol Chem 281:29739–29752. https://doi.org/10.1074/jbc.M600933200
3. Angelopoulou E, Bozi M, Simitsi A-M, Koros C, Antonelou R, Papagiannakis N et al (2022) Clinical differences between early-onset and mid-and-late-onset Parkinson's disease: data analysis of the Hellenic Biobank of Parkinson's disease. J Neurol Sci 442:120405. https://doi.org/10.1016/j.jns.2022.120405
4. Angelova PR, Esteras N, Evans J, Kostic M, Melki R, Prehn JHM et al (2025) α-synuclein fibrils per se but not α-synuclein seeded aggregation causes mitochondrial dysfunction and cell death in human neurons. Redox Biol 86:103817. https://doi.org/10.1016/j.redox.2025.103817
5. Bentivenga GM, Mammana A, Baiardi S, Rossi M, Ticca A, Magliocchetti F et al (2024) Performance of a seed amplification assay for misfolded alpha-synuclein in cerebrospinal fluid and brain tissue in relation to lewy body disease stage and pathology burden. Acta Neuropathol 147:18. https://doi.org/10.1007/s00401-023-02663-0
6. Braak H, Braak E (1991) Neuropathological stageing of Alzheimer-related changes. Acta Neuropathol 82:239–259. https://doi.org/10.1007/BF00308809
7. Braun AR, Liao EE, Horvath M, Kalra P, Acosta K, Young MC et al (2021) Potent inhibitors of toxic alpha-synuclein identified via cellular time-resolved FRET biosensors. NPJ Parkinsons Dis 7:52. https://doi.org/10.1038/s41531-021-00195-6
8. Bregendahl M, Kaya ZB, Singer W, McLean PJ (2025) Alpha-synuclein seeding amplification assays in Lewy body dementia: a brief review. Mol Neurodegener 20:77. https://doi.org/10.1186/s13024-025-00868-3
9. Chopra A, Lang AE, Höglinger G, Outeiro TF (2024) Towards a biological diagnosis of PD. Parkinsonism Relat Disord 122:106078. https://doi.org/10.1016/j.parkreldis.2024.106078
10. Davis AA, Inman CE, Wargel ZM, Dube U, Freeberg BM, Galluppi A et al (2020) APOE genotype regulates pathology and disease progression in synucleinopathy. Science Translational Medicine 12:eaay3069. https://doi.org/10.1126/scitranslmed.aay3069
11. De Luca CMG, Elia AE, Portaleone SM, Cazzaniga FA, Rossi M, Bistaffa E et al (2019) Efficient RT-QuIC seeding activity for α-synuclein in olfactory mucosa samples of patients with Parkinson's disease and multiple system atrophy. Transl Neurodegener 8:24. https://doi.org/10.1186/s40035-019-0164-x
12. Dickson DW (2018) Neuropathology of Parkinson disease. Parkinsonism Relat Disord 46:S30–S33. https://doi.org/10.1016/j.parkreldis.2017.07.033
13. Dickson DW (2012) Parkinson's disease and parkinsonism: neuropathology. Cold Spring Harb Perspect Med. https://doi.org/10.1101/cshperspect.a009258
14. Dujardin S, Commins C, Lathuiliere A, Beerepoot P, Fernandes AR, Kamath TV et al (2020) Tau molecular diversity contributes to clinical heterogeneity in Alzheimer's disease. Nat Med 26:1256–1263. https://doi.org/10.1038/s41591-020-0938-9
15. Farrow SL, Cooper AA, O'Sullivan JM (2022) Redefining the hypotheses driving Parkinson's diseases research. npj Parkinsons Dis 8:45. https://doi.org/10.1038/s41531-022-00307-w
16. Frieg B, Geraets JA, Strohäker T, Dienemann C, Mavroeidi P, Jung BC et al (2022) Quaternary structure of patient-homogenate amplified α-synuclein fibrils modulates seeding of endogenous α-synuclein. Commun Biol 5:1040. https://doi.org/10.1038/s42003-022-03948-y
17. Fujiwara H, Hasegawa M, Dohmae N, Kawashima A, Masliah E, Goldberg MS et al (2002) α-Synuclein is phosphorylated in synucleinopathy lesions. Nat Cell Biol 4:160–164. https://doi.org/10.1038/ncb748
18. Furman JL, Holmes BB, Diamond MI (2015) Sensitive detection of proteopathic seeding activity with fret flow cytometry. J Vis Exp. https://doi.org/10.3791/53205
19. Gerasimenko M, Yi H, Gilliland T, Chen Y, Wang Z, Zou WQ (2026) Biochemical signatures of skin α-synuclein in synucleinopathies revealed by RT-QuIC assay end-product analysis. Acta Neuropathol 151:3. https://doi.org/10.1007/s00401-025-02973-5
20. Ghanem SS, Majbour NK, Vaikath NN, Ardah MT, Erskine D, Jensen NM et al (2022) α-Synuclein phosphorylation at serine 129 occurs after initial protein deposition and inhibits seeded fibril formation and toxicity. Proc Natl Acad Sci U S A 119:e2109617119. https://doi.org/10.1073/pnas.2109617119

21. Goedert M, Spillantini MG, Del Tredici K, Braak H (2013) 100 years of Lewy pathology. Nat Rev Neurol 9:13–24. https://doi.org/10.1038/nrneurol.2012.242
22. Hähnel T, Raschka T, Sapienza S, Klucken J, Glaab E, Corvol J-C et al (2024) Progression subtypes in Parkinson's disease identified by a data-driven multi cohort analysis. npj Parkinsons Dis 10:95. https://doi.org/10.1038/s41531-024-00712-3
23. Hassanzadeh K, Liu J, Maddila S, Mouradian MM (2024) Post-translational modifications of α-synuclein, their therapeutic potential, and crosstalk in health and neurodegenerative diseases. Pharmacol Rev 76:1254–1290. https://doi.org/10.1124/pharmrev.123.001111
24. Hijaz BA, Volpicelli-Daley LA (2020) Initiation and propagation of α-synuclein aggregation in the nervous system. Mol Neurodegener 15:19. https://doi.org/10.1186/s13024-020-00368-6
25. Höglinger GU, Adler CH, Berg D, Klein C, Outeiro TF, Poewe W et al (2024) A biological classification of Parkinson's disease: the SynNeurGe research diagnostic criteria. Lancet Neurol 23:191–204. https://doi.org/10.1016/S1474-4422(23)00404-0
26. Höglinger GU, Lang AE (2025) SynNeurGe: the road ahead for a biological definition of Parkinson's disease. J Parkinsons Dis 15:931–938. https://doi.org/10.1177/1877718x241298194
27. Holmes BB, Furman JL, Mahan TE, Yamasaki TR, Mirbaha H, Eades WC et al (2014) Proteopathic tau seeding predicts tauopathy in vivo. Proc Natl Acad Sci U S A 111:E4376–E4385. https://doi.org/10.1073/pnas.1411649111
28. Jin Y, Li F, Sonoustoun B, Kondru NC, Martens YA, Qiao W et al (2022) APOE4 exacerbates α-synuclein seeding activity and contributes to neurotoxicity in Alzheimer's disease with Lewy body pathology. Acta Neuropathol 143:641–662. https://doi.org/10.1007/s00401-022-02421-8
29. Kolicheski A, Turcano P, Tamvaka N, McLean PJ, Springer W, Savica R et al (2022) Early-onset Parkinson's disease: creating the right environment for a genetic disorder. J Parkinsons Dis 12:2353–2367. https://doi.org/10.3233/jpd-223380
30. Lau A, So RWL, Lau HHC, Sang JC, Ruiz-Riquelme A, Fleck SC et al (2020) α-Synuclein strains target distinct brain regions and cell types. Nat Neurosci 23:21–31. https://doi.org/10.1038/s41593-019-0541-x
31. Lee SS, Civitelli L, Parkkinen L (2024) Brain-derived and in vitro-seeded alpha-synuclein fibrils exhibit distinct biophysical profiles. Elife 13:RP92775. https://doi.org/10.7554/eLife.92775
32. Lo CH (2021) Recent advances in cellular biosensor technology to investigate tau oligomerization. Bioeng Transl Med 6:e10231. https://doi.org/10.1002/btm2.10231
33. Lue LF, Walker DG, Adler CH, Shill H, Tran H, Akiyama H et al (2012) Biochemical increase in phosphorylated alpha-synuclein precedes histopathology of Lewy-type synucleinopathies. Brain Pathol 22:745–756. https://doi.org/10.1111/j.1750-3639.2012.00585.x
34. Maina KN, Smet-Nocca C, Bitan G (2023) Using FRET-based biosensor cells to study the seeding activity of Tau and α-synuclein. Methods Mol Biol 2551:125–145. https://doi.org/10.1007/978-1-0716-2597-2_10
35. Masuda-Suzukake M, Nonaka T, Hosokawa M, Oikawa T, Arai T, Akiyama H et al (2013) Prion-like spreading of pathological α-synuclein in brain. Brain 136:1128–1138. https://doi.org/10.1093/brain/awt037
36. Pang SY-Y, Ho PW-L, Liu H-F, Leung C-T, Li L, Chang EES et al (2019) The interplay of aging, genetics and environmental factors in the pathogenesis of Parkinson's disease. Transl Neurodegener 8:23. https://doi.org/10.1186/s40035-019-0165-9
37. Parra-Rivas LA, Madhivanan K, Aulston BD, Wang L, Prakashchand DD, Boyer NP et al (2023) Serine-129 phosphorylation of & #x3b1;-synuclein is an activity-dependent trigger for physiologic protein-protein interactions and synaptic function. Neuron 111:4006-4023.e4010. https://doi.org/10.1016/j.neuron.2023.11.020
38. Powers AE, Patel DS (2019) Expression and purification of untagged α-Synuclein. In: Bartels T (ed) Alpha-Synuclein: methods and protocols. Springer New York, City, pp 261–269
39. Prajjwal P, Flores Sanga HS, Acharya K, Tango T, John J, Rodriguez RSC et al (2023) Parkinson's disease updates: addressing the pathophysiology, risk factors, genetics, diagnosis, along with the medical and surgical treatment. Ann Med Surg Lond 85:4887–4902. https://doi.org/10.1097/ms9.0000000000001142
40. Pu J-L, Jin C-Y, Wang Z-X, Fang Y, Li Y-L, Xue N-J et al (2022) Apolipoprotein e genotype contributes to motor progression in Parkinson's disease. Mov Disord 37:196–200. https://doi.org/10.1002/mds.28805
41. Ramalingam N, Dettmer U (2023) α-Synuclein serine129 phosphorylation – the physiology of pathology. Mol Neurodegener 18:84. https://doi.org/10.1186/s13024-023-00680-x
42. Ramalingam N, Jin S-X, Moors TE, Fonseca-Ornelas L, Shimanaka K, Lei S et al (2023) Dynamic physiological α-synuclein S129 phosphorylation is driven by neuronal activity. npj Parkinsons Dis 9:4. https://doi.org/10.1038/s41531-023-00444-w
43. Reyes NGD, Pajo AT, Saranza G, Höglinger GU, Lang AE (2025) Revisiting Parkinson's disease definition and classification: insights from two emerging biological frameworks. J Neural Transm. https://doi.org/10.1007/s00702-025-03013-y
44. Riboldi GM, Frattini E, Monfrini E, Frucht SJ, Di Fonzo A (2021) A practical approach to Early-Onset Parkinsonism. J Parkinsons Dis 12:1–26. https://doi.org/10.3233/jpd-212815
45. Schneider SA, Alcalay RN (2017) Neuropathology of genetic synucleinopathies with parkinsonism: review of the literature. Mov Disord 32:1504–1523. https://doi.org/10.1002/mds.27193
46. Sekiya H, Franke L, Ono D, DeTure M, Ross OA, Murray ME et al (2025) Impact of hippocampal α-synuclein oligomers on cognitive trajectory in patients with dementia with Lewy bodies. Alzheimers Dement 21:e70374. https://doi.org/10.1002/alz.70374
47. Sekiya H, Tipton PW, Kawazoe M, Koga S, Murakami A, Maier AR et al (2024) Current landscape of clinical diagnosis in Multiple System Atrophy. Neurology 103:e210021. https://doi.org/10.1212/WNL.0000000000210021
48. Sekiya H, Tsuji A, Hashimoto Y, Takata M, Koga S, Nishida K et al (2022) Discrepancy between distribution of alpha-synuclein oligomers and Lewy-related pathology in Parkinson's disease. Acta Neuropathol Commun 10:133. https://doi.org/10.1186/s40478-022-01440-6
49. Shahnawaz M, Mukherjee A, Pritzkow S, Mendez N, Rabadia P, Liu X et al (2020) Discriminating α-synuclein strains in Parkinson's disease and multiple system atrophy. Nature 578:273–277. https://doi.org/10.1038/s41586-020-1984-7
50. Strohäker T, Jung BC, Liou S-H, Fernandez CO, Riedel D, Becker S et al (2019) Structural heterogeneity of α-synuclein fibrils amplified from patient brain extracts. Nat Commun 10:5535. https://doi.org/10.1038/s41467-019-13564-w
51. Su C, Hou Y, Xu J, Xu Z, Zhou M, Ke A et al (2024) Identification of Parkinson's disease PACE subtypes and repurposing treatments through integrative analyses of multimodal data. npj Digit Med 7:184. https://doi.org/10.1038/s41746-024-01175-9
52. Su D, Cui Y, He C, Yin P, Bai R, Zhu J et al (2025) Projections for prevalence of Parkinson's disease and its driving factors in 195 countries and territories to 2050: modelling study of Global Burden of Disease Study 2021. BMJ 388:e080952. https://doi.org/10.1136/bmj-2024-080952
53. Thal DR, Rüb U, Orantes M, Braak H (2002) Phases of Aβ-deposition in the human brain and its relevance for the development of AD. Neurology 58:1791–1800. https://doi.org/10.1212/WNL.58.12.1791

54. Van der Perren A, Gelders G, Fenyi A, Bousset L, Brito F, Peelaerts W et al (2020) The structural differences between patient-derived α-synuclein strains dictate characteristics of Parkinson's disease, multiple system atrophy and dementia with Lewy bodies. Acta Neuropathol 139:977–1000. https://doi.org/10.1007/s00401-020-02157-3
55. Walker DG, Lue L-F, Adler CH, Shill HA, Caviness JN, Sabbagh MN et al (2013) Changes in properties of serine 129 phosphorylated α-synuclein with progression of Lewy-type histopathology in human brains. Exp Neurol 240:190–204. https://doi.org/10.1016/j.expneurol.2012.11.020
56. Wang F, Banerjee V, Barria C, Ramirez S, Allison T, Gorski D et al (2025) Seed amplification of MSA alpha-synuclein aggregates preserves the biological and structural properties of brain-derived aggregates. Nat Commun 16:11266. https://doi.org/10.1038/s41467-025-66146-4
57. Wang Z, Li L, Xu Q, Pan H, Wang Y, Long Q et al (2025) The APOE ε4 allele affects the survival of patients with Parkinson's disease independent of dementia. J Transl Med 23:1094. https://doi.org/10.1186/s12967-025-07169-9
58. Wiseman JA, Turner CP, Faull RLM, Halliday GM, Dieriks BV (2025) Refining α-synuclein seed amplification assays to distinguish Parkinson's disease from multiple system atrophy. Transl Neurodegener 14:7. https://doi.org/10.1186/s40035-025-00469-6
59. Wojewska MJ, Otero-Jimenez M, Guijarro-Nuez J, Alegre-Abarrategui J (2023) Beyond strains: molecular diversity in alpha-synuclein at the center of disease heterogeneity. Int J Mol Sci 24:13199
60. Wüllner U, Borghammer P, Choe C-u, Csoti I, Falkenburger B, Gasser T et al (2023) The heterogeneity of Parkinson's disease. J Neural Transm 130:827–838. https://doi.org/10.1007/s00702-023-02635-4
61. Yamasaki TR, Holmes BB, Furman JL, Dhavale DD, Su BW, Song E-S et al (2019) Parkinson's disease and multiple system atrophy have distinct α-synuclein seed characteristics. J Biol Chem 294:1045–1058. https://doi.org/10.1074/jbc.RA118.004471
62. Zhao N, Attrebi ON, Ren Y, Qiao W, Sonustun B, Martens YA et al (2020) APOE4 exacerbates α-synuclein pathology and related toxicity independent of amyloid. Sci Transl Med. https://doi.org/10.1126/scitranslmed.aay1809